Table 2.5.3.5. *Symmetries of hexagonal six-beam CBED patterns for diffraction groups*

		Projection diffraction group										
		31_R		$3m1_R$						61_R		
Diffraction group		3	31_R	$3m_R$		$3m$		$3m1_R$		6	6_R	61_R
Two-dimensional symmetry		3	3	3		$3m$		$3m$		6	3	6
Three-dimensional symmetry			m'	$2'$				m', $(2')$			i	m', (i)
Zone-axis pattern	Bright-field pattern	3	6	$3m$		$3m$		$6mm$		6	3	6
	Whole-field pattern	3	3	3		$3m$		$3m$		6	3	6
Hexagonal six-beam pattern	O	1	1	1	m_2	1	m_v	m_2	m_v	1	1	1
	G	1	1_R	m_2	1	1	m_v	1_R	$1_R m_v(m_2)$	1	1	1_R
	F	1	1	m_2	1	1	1	1	m_2	1	1	1
	S	1	1	1	m_2	1	1	m_2	1	1	1	1
	FF'	1	3_R	1	1	1	m_v	3_R	$3_R m_v$	1	1	3_R
	SS'	1	1	1	1	1	m_v	1	m_v	1	6_R	6_R
A pair of symmetrical six-beam patterns 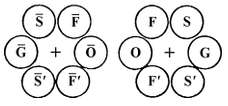	$\pm O$	1	1_R	m_2	1	m_v	1	$m_v 1_R$	$1_R m_2$	2	1	$2(1_R)$
	$\pm G$	1	1	1	m_R	m_v	1	$m_v m_R$	1	2	2_R	21_R
	$\pm F$	1	1	1	1	m_v	1	m_v	1	1	6_R	6_R
	$\pm S$	1	3_R	1	1	m_v	1	$3_R m_v$	3_R	1	1	3_R
	$F'\bar{F}$	1	1	1	m_R	1	1	m_R	1	2	1	2
	$S'\bar{S}$	1	1	m_R	1	1	1	1	m_R	2	1	2
Point group		23, 3	$\bar{6}$	432, 32		$\bar{4}3m$, $3m$		$\bar{6}m2$		6	$m3$, 3	$6/m$

		Projection diffraction group				
		$6mm1_R$				
Diffraction group		$6m_R m_R$	$6mm$	$6_R mm_R$		$6mm1_R$
Two-dimensional symmetry		6	$6mm$	$3m$		$6mm$
Three-dimensional symmetry		$2'$		i, $(2')$		m', $(i, 2')$
Zone-axis pattern	Bright-field pattern	$6mm$	$6mm$	$3m$		$6mm$
	Whole-field pattern	6	$6mm$	$3m$		$6mm$
Hexagonal six-beam pattern	O	m_2	m_v	1	$m_v(m_2)$	$m_v(m_2)$
	G	m_2	m_v	m_2	m_v	$1_R m_v(m_2)$
	F	m_2	1	m_2	1	m_2
	S	m_2	1	1	m_2	m_2
	FF'	1	m_v	1	m_v	$3_R m_v$
	SS'	1	m_v	6_R	$6_R m_v$	$6_R m_v$
A pair of symmetrical six-beam patterns 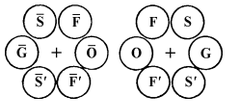	$\pm O$	$2m_2$	$2m_{v'}$	$m_v(m_2)$	1	$2(1_R)m_{v'}(m_2)$
	$\pm G$	$2m_R$	$2m_{v'}$	$2_R m_v$	$2_R m_R$	$21_R m_{v'}(m_R)$
	$\pm F$	1	$m_{v'}$	$6_R m_v$	6_R	$6_R m_{v'}$
	$\pm S$	1	$m_{v'}$	m_v	1	$3_R m_{v'}$
	$F'\bar{F}$	$2m_R$	2	1	m_R	$2m_R$
	$S'\bar{S}$	$2m_R$	2	m_R	1	$2m_R$
Point group		622	$6mm$	$m3m$, $\bar{3}m$		$6/mmm$

SMB pattern, and two-dimensional symmetry elements from a pair of SMB patterns, as shown in Tables 2.5.3.5, 2.5.3.6 and 2.5.3.7. Therefore, the use of a ZAP and SMB patterns is the most efficient way to find as many crystal symmetry elements in a specimen as possible.

2.5.3.3. Space-group determination

2.5.3.3.1. Lattice-type determination

When the point group of a specimen crystal is determined, the crystal axes may be found from a spot diffraction pattern recorded at a high-symmetry zone axis, using the orientations of the symmetry elements determined in the course of point-group determination. Integral-number indices are assigned to the spots of the diffraction patterns. The systematic absence of reflections indicates the lattice type of the crystal. It should be noted that reflections forbidden by the lattice type are always absent, even if dynamical diffraction takes place. (This is true for all sample thicknesses and accelerating voltages.) By comparing the experimentally obtained absences and the extinction rules known for the lattice types [P, C (A, B), I, F and R], a lattice type may be identified for the crystal concerned.

2.5.3.3.2. Identification of screw axes and glide planes

There are three space-group symmetry elements of diperiodic plane figures: (1) a horizontal screw axis $2'_1$, (2) a vertical glide plane g with a horizontal glide vector and (3) a horizontal glide plane g'. These are related to the point-group symmetry elements $2'$, m and m' of diperiodic plane figures, respectively. (It is noted that these symmetry elements and ten point-group symmetry elements form 80 space groups.)

Table 2.5.3.6. *Symmetries of square four-beam CBED patterns for diffraction groups*

			Projection diffraction group							
			41_R			$4mm1_R$				
Diffraction group			4	4_R	41_R	$4m_Rm_R$	$4mm$	4_Rmm_R		$4mm1_R$
Two-dimensional symmetry			4	(2)	4	4	$4mm$	($2mm$)		$4mm$
Three-dimensional symmetry				$\bar{4}$	m', (i, $\bar{4}$)	$2'$		$\bar{4}$, $2'$		m', (i, $2'$, $\bar{4}$)
Zone-axis pattern	Bright-field pattern		4	4	4	$4mm$	$4mm$	$4mm$		$4mm$
	Whole-field pattern		4	2	4	4	$4mm$	$2mm$		$4mm$
Square four-beam pattern		O	1	1	1	m_2	m_v	m_2	m_v	$m_v(m_2)$
		G	1	1	1_R	m_2	m_v	m_2	m_v	$1_Rm_v(m_2)$
		F	1	1	1	m_2	1	1	m_2	m_2
		FF'	1	4_R	4_R	1	m_v	4_R	4_Rm_v	4_Rm_v
Two pairs of square four-beam patterns 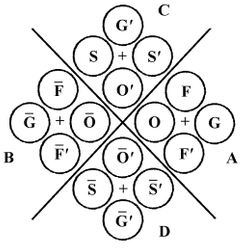	AB	$\pm O$	2	2	$2(1_R)$	$2m_2$	$2m_{v'}$	$2m_2$	$2m_{v'}$	$2(1_R)m_{v'}(m_2)$
		$\pm G$	2	2	21_R	$2m_R$	$2m_{v'}$	$2m_R$	$2m_{v'}$	$21_Rm_{v'}(m_R)$
		FF'	2	2	2	$2m_R$	2	2	$2m_R$	$2m_R$
		$\pm F$	1	4_R	4_R	1	$m_{v'}$	4_R	$4_Rm_{v'}$	$4_Rm_{v'}$
	AC	OO'	4	4	4	$4m_2$	$4m_{v''}$	$4m_v$	$4m_2$	$4m_{v''}(m_2)$
		GG'	4	4_R	41_R	$4m_R$	$4m_{v''}$	4_Rm_v	4_Rm_R	$41_Rm_{v''}(m_R)$
		FS	4	1	4	$4m_R$	4	m_R	1	$41_Rm_{v''}(m_R)$
		FS'	1	1	1_R	1	$m_{v''}$	m_v	1	$1_Rm_{v''}$
Point group			4	$\bar{4}$	$4/m$	432, 422	$4mm$	$\bar{4}3m$, $\bar{4}2m$		$m3m$, $4/mmm$

Table 2.5.3.7. *Symmetries of rectangular four-beam CBED patterns for diffraction groups*

			Projection diffraction group						
			$m1_R$			$2mm1_R$			
Diffraction group			m_R	m	$m1_R$	$2m_Rm_R$	$2mm$	2_Rmm_R	$2mm1_R$
Two-dimensional symmetry				m	m	2	$2mm$	m	$2mm$
Three-dimensional symmetry			$2'$		m', $2'$	$2'$		$2'$, i	m', $2'$, i
Zone-axis pattern	Bright-field pattern		m	m	$2mm$	$2mm$	$2mm$	m	$2mm$
	Whole-field pattern		1	m	m	2	$2mm$	m	$2mm$
Rectangular four-beam pattern		O	1	1	1	1	1	1	1
		G	1	1	1_R	1	1	1	1_R
		F	m_2	1	m_2	m_2	1	m_2	m_2
		S	1	1	1	m_2	1	1	m_2
Three pairs of rectangular four-beam patterns 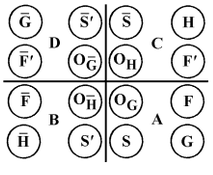	AB	$O_GO_{\bar{H}}$	m_2	1	m_2	m_2	m_v	$m_v(m_2)$	$m_v(m_2)$
		$G\bar{H}$	1	1	1	m_R	m_v	m_v	m_vm_R
		$F\bar{F}$	1	1	1	1	m_v	2_Rm_v	2_Rm_v
		SS'	1	1	1_R	1	m_v	m_v	m_v1_R
	AC	O_GO_H	1	m_v	m_v	m_2	$m_{v'}$	1	$m_{v'}(m_2)$
		GH	m_R	m_v	m_vm_R	m_R	$m_{v'}$	m_R	$m_{v'}m_R$
		FF'	1	m_v	m_v1_R	1	$m_{v'}$	1	$m_{v'}1_R$
		$S\bar{S}$	1	m_v	m_v	1	$m_{v'}$	2_R	$2_Rm_{v'}$
	AD	$O_GO_{\bar{G}}$	1	1	1_R	2	2	1	$2(1_R)$
		GG	1	1	1	2	2	2_R	21_R
		$F\bar{F}'$	1	1	1	$2m_R$	2	1	$2m_R$
		$S\bar{S}'$	m_R	1	m_R	$2m_R$	2	m_R	$2m_R$
Point group			2, 222, $mm2$, 4, $\bar{4}$, 422, $4mm$, $\bar{4}2m$, 32, $\bar{6}$, 622, $6mm$, $\bar{6}m2$, 23, 432, $\bar{4}3m$	m, $mm2$, $4mm$, $\bar{4}2m$, $3m$, $\bar{6}$, $6mm$, $\bar{6}m2$, $\bar{4}3m$	$mm2$, $4mm$, $42m$, $6mm$, $\bar{6}m2$, $\bar{4}3m$	222, 422, $\bar{4}2m$, 622, 23, 432	$mm2$, $\bar{6}m2$	$2/m$, mmm, $4/m$, $4/mmm$, $\bar{3}m$, $\bar{6}/m$, $6/mmm$, $m3$, $m3m$	mmm, $4/mmm$, $m3$, $m3m$, $6/mmm$

The ordinary extinction rules for screw axes and glide planes hold only in the approximation of kinematical diffraction. The kinematically forbidden reflections caused by these symmetry elements appear owing to *Umweganregung* of dynamical diffraction. Extinction of intensity, however, does take place in these reflections at certain crystal orientations with respect to the incident beam (*i.e.* in certain regions within a CBED disc). This dynamical extinction was first predicted by Cowley & Moodie (1959) and was discussed by Miyake *et al.* (1960) and Cowley *et al.* (1961). Goodman & Lehmpfuhl (1964) first observed the dynamical extinction as dark cross lines in kinematically forbidden reflection discs of CBED patterns of CdS. Gjønnes & Moodie

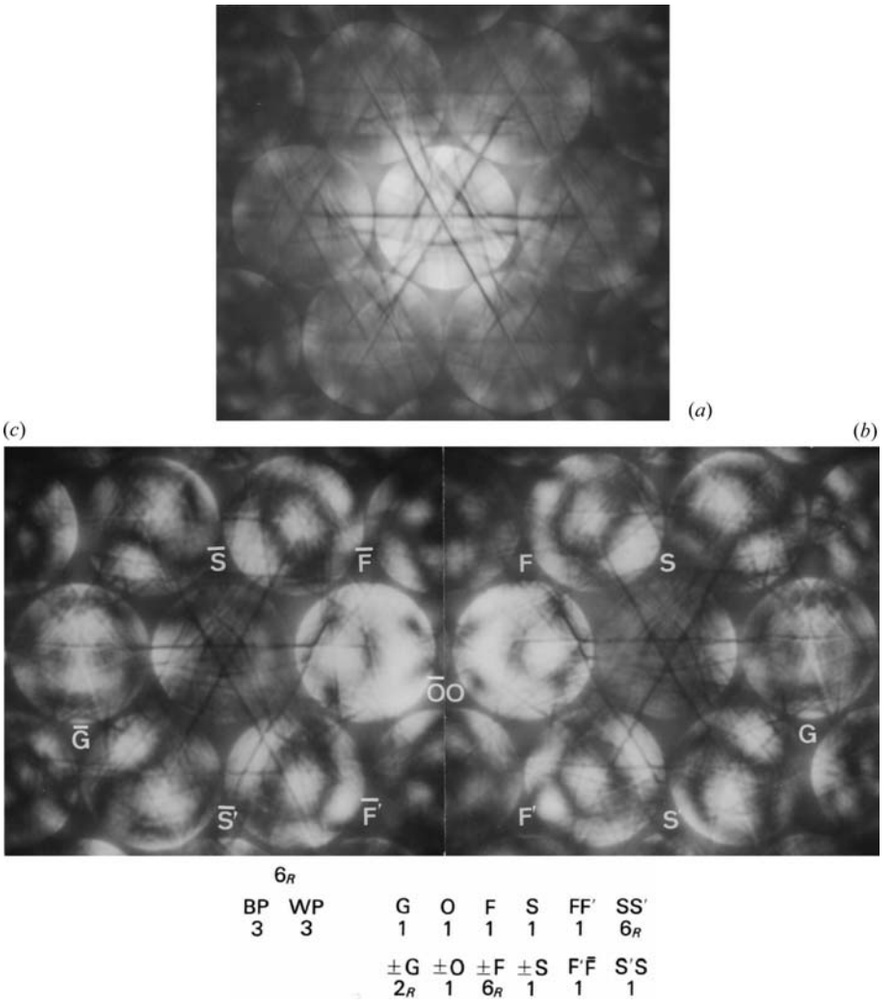

Fig. 2.5.3.8. CBED patterns of FeS_2 taken with the [111] incidence. (*a*) Zone-axis pattern, (*b*) hexagonal six-beam pattern with excitation of reflection $+G$, (*c*) hexagonal six-beam pattern with excitation of reflection $-G$. Symmetry 6_R is noted between discs S and S' and discs $\bar{F}$ and $\bar{F}'$.

(1965) discussed the dynamical extinction in a more general way considering not only ZOLZ reflections but also HOLZ reflections. They completely clarified the dynamical extinction rules by considering the exact cancellation which may occur along certain symmetry-related multiple-scattering paths. Based on the results of Gjønnes & Moodie (1965), Tanaka, Sekii & Nagasawa (1983) tabulated the dynamical extinctions expected at all the possible crystal orientations for all the space groups. These were later tabulated in a better form on pages 162 to 172 of the book by Tanaka & Terauchi (1985).

Fig. 2.5.3.10(*a*) illustrates *Umweganregung* paths to a kinematically forbidden reflection. The $0k0$ (k = odd) reflections are kinematically forbidden because a b-glide plane exists perpendicular to the a axis and/or a 2_1 screw axis exists in the b direction. Let us consider an *Umweganregung* path a in the zeroth-order Laue zone to the 010 forbidden reflection and path b which is symmetric to path a with respect to axis k. Owing to the translation of one half of the lattice parameter b caused by the glide plane and/or the 2_1 screw axis, the following relations hold between the crystal structure factors:

$$F(h,k) = F(\bar{h},k) \quad \text{for } k = 2n,$$
$$F(h,k) = -F(\bar{h},k) \quad \text{for } k = 2n+1. \qquad (2.5.3.1)$$

That is, the structure factors of reflections $hk0$ and $\bar{h}k0$ have the same phase for even k but have opposite phases for odd k.

Since an *Umweganregung* path to the kinematically forbidden reflection $0k0$ contains an odd number of reflections with odd k, the following relations hold:

$$F(h_1,k_1)F(h_2,k_2)\ldots F(h_n,k_n) \quad \text{for path } a$$
$$= -F(\bar{h}_1,k_1)F(\bar{h}_2,k_2)\ldots F(\bar{h}_n,k_n) \quad \text{for path } b, \qquad (2.5.3.2)$$

where

$$\sum_{i=1}^{n} h_i = 0, \quad \sum_{i=1}^{n} k_i = k \ (k = \text{odd})$$

and the functions including the excitation errors are omitted because only the cases in which the functions are the same for all the paths are considered. The excitation errors for paths a and b become the same when the projection of the Laue point along the zone axis concerned, L, lies on axis k. Since the two waves passing through paths a and b have the same amplitude but opposite signs, these waves are superposed on the $0k0$ discs (k = odd) and cancel out, resulting in dark lines A in the forbidden discs, as shown in Fig. 2.5.3.10(*b*). The line A runs parallel to axis k passing through the projection point of the zone axis.

In path c, the reflections are arranged in the reverse order to those in path b. When the 010 reflection is exactly excited, two paths a and c are symmetric with respect to the bisector m'–m' of

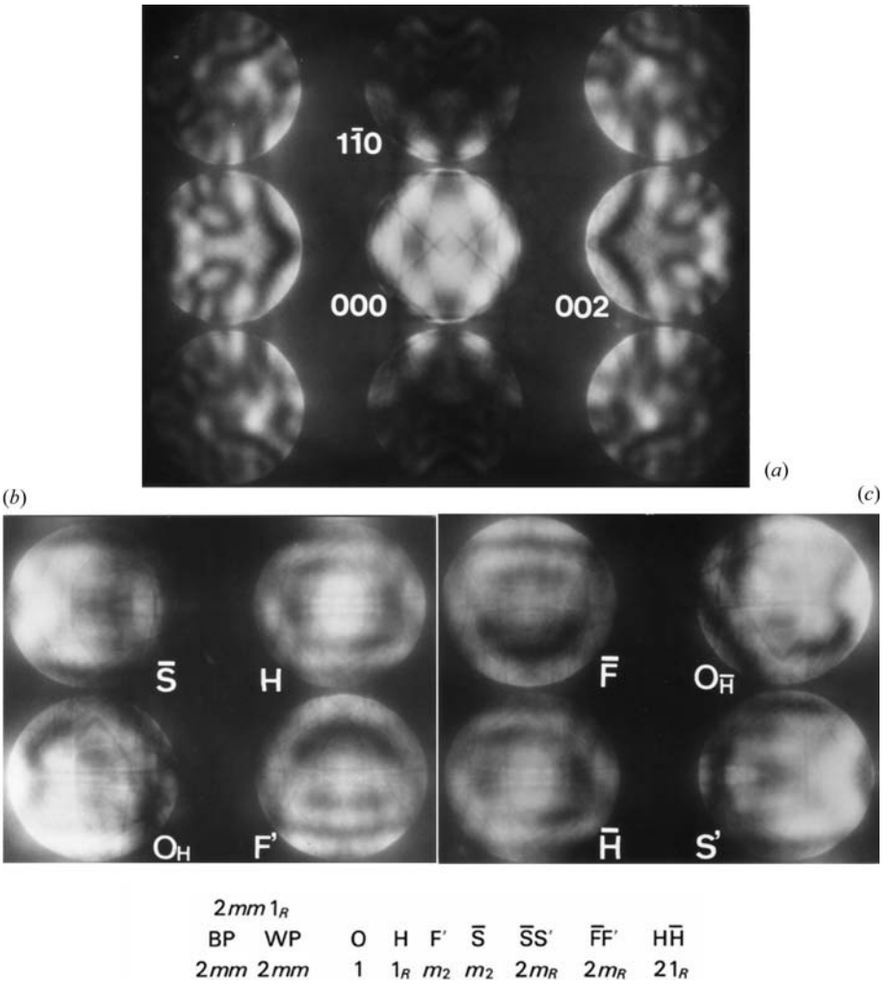

Fig. 2.5.3.9. CBED patterns of V_3Si taken with the [110] incidence. (*a*) Zone-axis pattern, (*b*) rectangular four-beam pattern with excitation of reflections H, $\bar{S}$ and F, (*c*) rectangular four-beam pattern with excitation of reflections $\bar{H}$, S and $\bar{F}$.

the 010 vector having the same excitation errors. The following equation holds:

$$F(h_1, k_1)F(h_2, k_2)\ldots F(h_n, k_n) \quad \text{for path } a$$
$$= -F(\bar{h}_n, k_n)F(\bar{h}_{n-1}, k_{n-1})\ldots F(\bar{h}_1, k_1) \quad \text{for path } c. \tag{2.5.3.3}$$

Since the waves passing through these paths have the same amplitude but opposite signs, these waves are superposed on the 010 discs and cancel out, resulting in dark line B in this disc, as shown in Fig. 2.5.3.10(*b*). Line B appears perpendicular to line A at the exact Bragg positions. When *Umweganregung* paths are present only in the zeroth-order Laue zone, the glide plane and screw axis produce the same dynamical extinction lines A and B. We call these lines A_2 and B_2 lines, subscript 2 indicating that the *Umweganregung* paths lie in the zeroth-order Laue zone.

The dynamical extinction effect is analogous to interference phenomena in the Michelson interferometer. That is, the incident beam is split into two beams by Bragg reflections in a crystal. These beams take different paths, in which they suffer a relative phase shift of π and are finally superposed on a kinematically forbidden reflection to cancel out.

When the paths include higher-order Laue zones, the glide plane produces only extinction lines A but the screw axis causes only extinction lines B. These facts are attributed to the different relations between structure factors for a 2_1 screw axis and a glide plane,

$$F(hkl) = (-1)^k F(\bar{h}k\bar{l}) \quad \text{for a } 2_1 \text{ screw axis in the [010] direction,} \tag{2.5.3.4}$$

$$F(hkl) = (-1)^k F(\bar{h}kl) \quad \text{for a } b \text{ glide in the (100) plane.} \tag{2.5.3.5}$$

In the case of the glide plane, extinction lines A are still formed because two waves passing through paths a and b have opposite signs to each other according to equation (2.5.3.5), but extinction lines B are not produced because equation (2.5.3.4) holds only for the 2_1 screw axis. In the case of the 2_1 screw axis, only the waves passing through paths a and c have opposite signs according to equation (2.5.3.4), forming extinction lines B only. We call these lines A_3 and B_3 dynamical extinction lines, suffix 3 indicating the *Umweganregung* paths being *via* higher-order Laue zones.

It was predicted by Gjønnes & Moodie (1965) that a horizontal glide plane g' gives a dark spot at the crossing point between extinction lines A and B (Fig. 2.5.3.10*b*) due to the cancellation between the waves passing through paths b and c. Tanaka, Terauchi & Sekii (1987) observed this dynamical extinction, though it appeared in a slightly different manner to that predicted by Gjønnes & Moodie (1965). Table 2.5.3.8 summarizes the appearance of the dynamical extinction lines for the glide planes g and g' and the 2_1 screw axis. The three space-group symmetry elements can be identified from the observed extinctions because these three symmetry elements produce different kinds of dynamical extinctions.

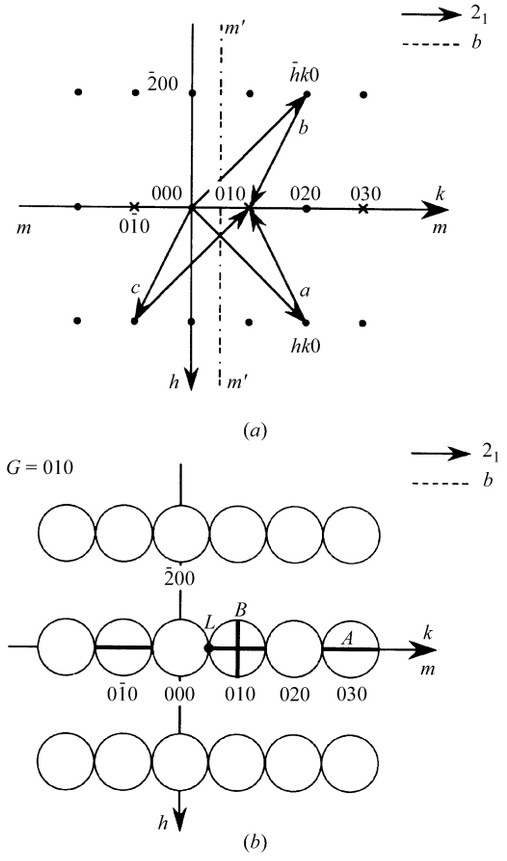

Fig. 2.5.3.10. Illustration of the production of dynamical extinction lines in kinematically forbidden reflections due to a b-glide plane and a 2_1 screw axis. (a) *Umweganregung* paths a, b and c. (b) Dynamical extinction lines A are formed in forbidden reflections $0k0$ (k = odd). Extinction line B perpendicular to the lines A is formed in the exactly excited 010 reflection.

In principle, a horizontal screw axis and a vertical glide plane can be distinguished by observations of the extinction lines A_3 and B_3. It is, however, not easy to observe the extinction lines A_3 and B_3 because broad extinction lines A_2 and B_2 appear at the same time. The presence of the extinction lines A_3 and B_3 can be revealed by inspecting the symmetries of fine defect HOLZ lines appearing in the forbidden reflections instead of by direct observation of the lines A_3 and B_3 (Tanaka, Sekii & Nagasawa, 1983). That is, if HOLZ lines form lines A_3 and B_3, HOLZ lines are symmetric with respect to the extinction lines A_2 and B_2. If HOLZ lines do not form lines A_3 and B_3, HOLZ lines are asymmetric with respect to the extinction lines A_2 and B_2. When the HOLZ lines are symmetric about the extinction lines A_2, the specimen crystal has a glide plane. When the HOLZ lines are symmetric with respect to lines B_2, a 2_1 screw axis exists. It should

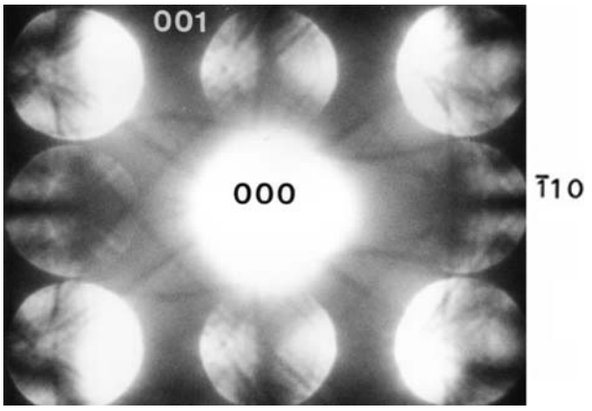

Fig. 2.5.3.12. CBED pattern of FeS_2 taken with the [110] electron-beam incidence. In the 001 and $00\bar{1}$ discs, HOLZ lines are asymmetric with respect to extinction lines A_2, indicating the existence of a 2_1 screw axis parallel to the c axis. In the $\bar{1}10$ and $1\bar{1}0$ discs, HOLZ lines are symmetric with respect to extinction lines A_2, indicating existence of a glide plane perpendicular to the c axis.

be noted that a relatively thick specimen area has to be selected to observe HOLZ lines in ZOLZ reflection discs.

Fig. 2.5.3.11 shows CBED patterns taken from (a) thin and (b) thick areas of FeS_2, whose space group is $P2_1/a\bar{3}$, at the 001 Bragg setting with the [100] electron-beam incidence. In the case of the thin specimen (Fig. 2.5.3.11a), only the broad dynamical extinction lines formed by the interaction of ZOLZ reflections are seen in the odd-order discs. On the other hand, fine HOLZ lines are clearly seen in the thick specimen (Fig. 2.5.3.11b). The HOLZ lines are symmetric with respect to both A_2 and B_2 extinction lines. This fact proves the presence of the extinction lines A_3 and B_3, or both the c glide in the (010) plane and the 2_1 screw axis in the c direction, this fact being confirmed by consulting Table 2.5.3.9. Fig. 2.5.3.12 shows a [110] zone-axis CBED pattern of FeS_2. A_2 extinction lines are seen in both the 001 and $\bar{1}10$ discs. Fine HOLZ lines are symmetric with respect to the A_2 extinction lines in the $\bar{1}10$ disc but asymmetric about the A_2 extinction line in the 001 disc, indicating formation of the A_3 extinction line only in the $\bar{1}10$ disc. This proves the existence of a 2_1 screw axis in the [001] direction and an a glide in the (001) plane. The appearance of HOLZ lines is easily changed by a change of a few hundred volts in the accelerating voltage. Steeds & Evans (1980) demonstrated for spinel changes in the appearance of HOLZ lines in the ZOLZ discs at accelerating voltages around 100 kV.

Another practical method for distinguishing between glide planes and 2_1 screw axes is that reported by Steeds *et al.* (1978). The method is based on the fact that the extinction lines are observable even when a crystal is rotated with a glide plane kept parallel and with a 2_1 screw axis perpendicular to the incident

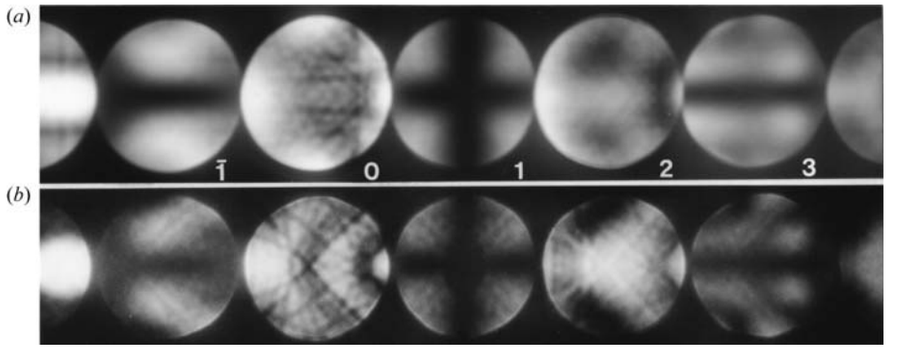

Fig. 2.5.3.11. CBED patterns obtained from (a) thin and (b) thick areas of (001) FeS_2. (a) Dynamical extinction lines A_2 and B_2 are seen. (b) Extinction lines A_3 and B_3 as well as A_2 and B_2 are formed because HOLZ lines are symmetric about lines A_2 and B_2.

Table 2.5.3.8. *Dynamical extinction rules for an infinitely extended parallel-sided specimen*

Symmetry elements of plane-parallel specimen	Orientation to specimen surface	Dynamical extinction lines	
		Two-dimensional (zeroth Laue zone) interaction	Three-dimensional (HOLZ) interaction
Glide planes	perpendicular: g	A_2 and B_2	A_3
	parallel: g'	—	intersection of A_3 and B_3
Twofold screw axis	perpendicular: 2_1	—	—
	parallel: $2_1'$	A_2 and B_2	B_3

beam. With reference to Fig. 2.5.3.10(*a*), extinction lines A_3 produced by a glide plane remain even when the crystal is rotated with respect to axis h but the lines are destroyed by a rotation of the crystal about axis k. Extinction lines B_3 originating from a 2_1 screw axis are not destroyed by a crystal rotation about axis k but the lines are destroyed by a rotation with respect to axis h.

2.5.3.3.3. Space-group determination

We now describe a space-group determination method which uses the dynamical extinction lines caused by the horizontal screw axis $2_1'$ and the vertical glide plane g of an infinitely extended parallel-sided specimen. We do not use the extinction due to the glide plane g' because observation of the extinction requires a laborious experiment. It should be noted that a vertical glide plane with a glide vector not parallel to the specimen surface cannot be a symmetry element of a specimen of finite thickness; however, the component of the glide vector perpendicular to the incident beam acts as a symmetry element g. (Which symmetry elements are observed by CBED is discussed in Section 2.5.3.3.5.) The 2_1, 4_1, 4_3, 6_1, 6_3 and 6_5 screw axes of crystal space groups that are set perpendicular to the incident beam act as a symmetry element $2_1'$ because two or three successive operations of 4_1, 4_3, 6_1, 6_3 and 6_5 screw axes make them equivalent to a 2_1 screw axis: $(4_1)^2 = (4_3)^2 = (6_1)^3 = (6_3)^3 = (6_5)^3 = 2_1$. The 4_2, 3_1, 3_2, 6_2 and 6_4 screw axes that are set perpendicular to the incident beam do not produce dynamical extinction lines because the 4_2 screw axis acts as a twofold rotation axis due to the relation $(4_2)^2 = 2$, the 3_1 and 3_2 screw axes give no specific symmetry in CBED patterns, and the 6_2 and 6_4 screw axes are equivalent to 3_1 and 3_2 screw axes due to the relations $(6_2)^2 = 3_2$ and $(6_4)^2 = 3_1$. Modifications of the dynamical extinction rules were investigated by Tanaka, Sekii & Nagasawa (1983) when more than one crystal symmetry element (that gives rise to dynamical extinction lines) coexists and when the symmetry elements are combined with various lattice types. Using these results, dynamical extinction lines A_2, A_3, B_2 and B_3 expected from all the possible crystal settings for all the space groups were tabulated.

Table 2.5.3.9 shows all the dynamical extinction lines appearing in the kinematically forbidden reflections for all the possible crystal settings of all the space groups. The first column gives space groups. In each of the following pairs of columns, the left-hand column of the pair gives the reflection indices and the symmetry elements causing the extinction lines and the right-hand column gives the types of the extinction lines. The (second) suffixes 1, 2 and 3 of a 2_1 screw axis in each column distinguish the first, the second and the third screw axis of the space group (as in the symbols 2_{11} and 2_{12} of space group $P2_12_12$). The glide symbols in the [001] column for space group $P4/nnc$ have two suffixes (n_{21} and n_{22}). The first suffix 2 denotes the second glide plane of the space group. The second suffixes 1 and 2, which appear in the tetragonal and cubic systems, distinguish two equivalent glide planes which lie in the x and y planes. The equivalent planes are distinguished only for the cases of [100], [010] and [001] electron-beam incidences, for convenience. The c-glide planes of space group $Pcc2$ are distinguished with symbols c_1 and c_2 (the first suffix only), because the equivalent planes do not exist. The glide symbol in the [001] column for space group $P4/mbm$ has only one suffix 1 or 2. The suffix distinguishes the equivalent glide planes lying in the x and y planes. The first suffix to distinguish the first and the second glide planes is not necessary because the space group has only one glide symbol b. When the index of the incident-beam direction is expressed with a symbol like $[h0l]$ for point groups 2, m and $2/m$, the index h or l can take a value of zero. That is, the extinction rules are applicable to the [100] and [001] electron-beam incidences. However, if columns for [100], [010] and [001] incidences are present, as in the case of point group $mm2$, $[hk0]$, $[0kl]$ and $[h0l]$ incidences are only for nonzero h, k and l. The reflections in which the extinction lines appear are always perpendicular to the corresponding incident-beam directions ($0k'l' \perp [0kl]$, $h'k'0 \perp [hk0]$, ...). The indices of the reflections in which extinction lines appear are odd if no remark is given. For c-glide planes of space groups $R3c$ and $R\bar{3}c$ and for d-glide planes, the reflections in which extinction lines appear are specified as $6n + 3$ and $4n + 2$ orders, respectively.

The number of indistinguishable space groups was first counted by Tanaka, Sekii & Nagasawa (1983) but later corrections were made by Eades & Spence (1987). It was found that 177 space groups out of 230 can be identified using the extinction lines (Tanaka *et al.*, 2002). Another reference for space-group determination is due to Eades (1988). The indistinguishable space-group sets using the extinction lines are listed in Table 2.5.3.10. Most of the sets are caused by the fact that CBED cannot identify 4_2, 3_1 (3_2) and 6_2 (6_4) screw axes. However, these sets can be rather easily distinguished in the ordinary way, that is, by observing how the intensities of the reflections which may be kinematically forbidden change when the crystal orientation is varied. If the axis concerned is a screw axis, kinematically forbidden reflections show a sudden decrease in intensity when an orientation change causes the loss of *Umweganregung* paths. If the axis is a rotation axis, the intensities of the reflections do not change conspicuously for such an orientation change. Using this test, each space group in the 23 sets can be identified except the pairs in parentheses and pairs (16) and (17) in Table 2.5.3.10 (see Eades, 1988).

Tsuda *et al.* (2000) showed theoretically that the coherent CBED method can distinguish between space groups ($I23$ and $I2_13$) and between ($I222$ and $I2_12_12_1$), which are indistinguishable pairs (16) and (17), respectively, in Table 2.5.3.10. The coherent CBED pattern is obtained in such a way that the convergence angle of the incident beam is set to a larger value than usual to make adjacent CBED discs overlap (Dowell & Goodman, 1973). When the focus point is displaced from the specimen, or a certain area is illuminated, sinusoidal interference fringes of the lattice spacing corresponding to the adjacent discs are formed in the overlapping regions if the probe size of the incident beam is smaller than the lattice spacing. (If the focus point of the incident beam is on the specimen, each overlapping region of the CBED discs shows uniform intensity.) Formation of the interference fringes was explained in detail first by Spence & Cowley (1978). Vine *et al.* (1992) showed distortion-free interference fringes from 6*H*-SiC and succeeded in observing the fringes with a shift of half a period due to a glide plane. Tsuda *et al.*'s method